materials

MDPI

Article

Annealing-Dependent Morphotropic Phase Boundary in the $BiMg_{0.5}Ti_{0.5}O_3$–$BiZn_{0.5}Ti_{0.5}O_3$ Perovskite System

João Pedro V. Cardoso [1], Vladimir V. Shvartsman [2,*], Anatoli V. Pushkarev [3], Yuriy V. Radyush [3], Nikolai M. Olekhnovich [3], Dmitry D. Khalyavin [4], Erik Čižmár [5], Alexander Feher [5] and Andrei N. Salak [1,*]

1 Department of Materials and Ceramics Engineering and CICECO—Aveiro Institute of Materials, University of Aveiro, 3810-193 Aveiro, Portugal
2 Institute for Materials Science and CENIDE—Centre for Nanointegration Duisburg-Essen, University of Duisburg-Essen, 45141 Essen, Germany
3 Scientific-Practical Materials Research Centre of NASB, 220072 Minsk, Belarus
4 ISIS Facility, Rutherford Appleton Laboratory, Chilton, Didcot, Oxfordshire OX11 0QX, UK
5 Institute of Physics, Faculty of Science, Pavol Jozef Šafárik University, 041 54 Košice, Slovakia
* Correspondence: vladimir.shvartsman@uni-due.de (V.V.S.); salak@ua.pt (A.N.S.)

Abstract: The annealing behavior of (1-x)$BiMg_{0.5}Ti_{0.5}O_3$–$xBiZn_{0.5}Ti_{0.5}O_3$ [(1-x)BMT–xBZT] perovskite solid solutions synthesized under high pressure was studied in situ via X-ray diffraction and piezoresponse force microscopy. The as prepared ceramics show a morphotropic phase boundary (MPB) between the non-polar orthorhombic and ferroelectric tetragonal states at 75 mol. % BZT. It is shown that annealing above 573 K results in irreversible changes in the phase diagram. Namely, for compositions with $0.2 < x < 0.6$, the initial orthorhombic phase transforms into a ferroelectric rhombohedral phase. The new MPB between the rhombohedral and tetragonal phases lies at a lower BZT content of 60 mol. %. The phase diagram of the BMT–BZT annealed ceramics is formally analogous to that of the commercial piezoelectric material lead zirconate titanate. This makes the BMT–BZT system promising for the development of environmentally friendly piezoelectric ceramics.

Keywords: lead-free; high-pressure synthesis; conversion polymorphism; X-ray diffraction; piezoresponse force microscopy

Citation: Cardoso, J.P.V.; Shvartsman, V.V.; Pushkarev, A.V.; Radyush, Y.V.; Olekhnovich, N.M.; Khalyavin, D.D.; Čižmár, E.; Feher, A.; Salak, A.N. Annealing-Dependent Morphotropic Phase Boundary in the $BiMg_{0.5}Ti_{0.5}O_3$–$BiZn_{0.5}Ti_{0.5}O_3$ Perovskite System. *Materials* **2022**, *15*, 6998. https://doi.org/10.3390/ma15196998

Academic Editors: Irena Jankowska-Sumara and Magdalena Krupska-Klimczak

Received: 14 September 2022
Accepted: 6 October 2022
Published: 9 October 2022

1. Introduction

Solid solutions of perovskite (anti)ferroelectric compounds and other multicomponent systems with continuously changeable chemical compositions have been of great interest for many decades. In such materials, there is a coexistence of different structural phases and phase boundaries, in which their dielectric permittivity and electromechanical coefficients achieve very high values. $PbZr_{1-x}Ti_xO_3$ (PZT) with the range of coexistence of several ferroelectric phases (morphotropic phase boundary, MPB) is an outstanding example [1–4]. It was generally accepted for a long time that MPB in this solid solution system separates the structural phases of rhombohedral (R) and tetragonal (T) symmetries and locates close to x = 0.47 at room temperature. In 1999, based on a precision synchrotron diffraction study, Noheda et al. [5,6] demonstrated that there is a monoclinic phase (M_A), located between R and T. In 2014, a detailed study using neutron powder diffraction carried out by Zhang et al. [7] has revealed another monoclinic phase (M_B) with a boundary to the M_A structural phase. It was shown that the intermediate monoclinic phase allows continuous change (rotation) of the polarization vector, and the large piezoelectric response of PZT at MPB can be associated with this effect [6]. The motion of the domain walls and the interphase boundaries in the external field was demonstrated to contribute to the induced polarization as well [8,9]. In relaxor ferroelectrics with MPB, such as $PbMg_{1/3}Nb_{2/3}O_3$–$PbTiO_3$ and $PbZn_{1/3}Nb_{2/3}O_3$–$PbTiO_3$, the movement (flipping

and breathing) of numerous neighboring polar nanoregions is the main mechanism that explains their very high electromechanical response [10,11].

Ecological requirements have stimulated a search for lead-free alternatives to the aforementioned piezoelectric materials. Solid solutions between well-known ferroelectrics and antiferroelectrics such as $BaTiO_3$, $NaNbO_3$, $KNbO_3$, $Na_{1/2}Bi_{1/2}TiO_3$ and $K_{1/2}Bi_{1/2}TiO_3$ were studied in this respect [12]. Some of the systems, e.g., $K_{1/2}Bi_{1/2}TiO_3$–$BaTiO_3$, which were found to be promising, are under intense study to enhance the electromechanical characteristics and adjust them to the operating range as well as to make the ceramics production process simpler and easily reproducible. At the same time, many efforts are focused on discovering new lead-free perovskite systems with MPB. Attempting to reveal new compositions, researchers explore multicomponent systems, in which one or more end members do not have a stable modification at ambient pressure (e.g., $BiScO_3$ [13], $BiMnO_3$ [14] and $BiCrO_3$ [15]). In some cases, the compositions corresponding to MPB in such systems can be prepared using conventional routes; the majority of cases require the application of high-pressure synthesis. Novel solid solution systems with MPB stabilized under high pressure have been reported [16–20]. In the MPB ranges of the $BiCo_{1-x}Fex O_3$ [17] and $Na_{1/2}Bi_{1/2}V_{1-x}Ti_xO_3$ [20] systems, a monoclinic phase with polarization rotation similar to that observed in PZT was detected.

In the (1-*x*)$BiMg_{0.5}Ti_{0.5}O_3$–*x*$BiZn_{0.5}Ti_{0.5}O_3$ system [(1-*x*)BMT–*x*BZT], in which the orthorhombic BMT is a structural analogue of $PbZrO_3$ [21], while the tetragonal BZT is isostructural to $PbTiO_3$ [22], neither the end members nor their solid solutions can be obtained in bulk form through conventional routes. The as-prepared (unannealed) compositions with a relative BZT content $x < 0.75$ are orthorhombic (space group *Pnnm*), while those with a BZT content above this value are tetragonal (*P*4*mm*). In the solution with $x = 0.75$, both phases coexist, forming an MPB [23].

A phenomenon of annealing-stimulated irreversible transformations of the high-pressure stabilized phases (conversion polymorphism) [24] has recently been revealed. It was shown that the pattern of the phase diagram of the high-pressure prepared complex perovskite compositions, which demonstrates the effect of conversion polymorphism, depends on the maximum annealing temperature. This feature can be used to design new materials with MPB since by means of controlled annealing, materials with different combinations of the perovskite phases can be obtained.

In this paper, we study the effect of annealing on the state of high-pressure sintered (1-*x*)BMT–*x*BZT ceramics with compositions around the MPB. We report on the in situ temperature X-ray diffraction study and the Piezoresponse Force Microscopy measurements of the (1-*x*)BMT–*x*BZT ceramics and demonstrate the annealing-stimulated irreversible changes in the structural phase diagram and in the polar domain structure of the ceramics. The phase diagram of the annealed BMT–BZT solid solutions is analyzed in comparison with that of PZT.

2. Materials and Methods

The (1-*x*)BMT–*x*BZT ceramics were produced using high-pressure high-temperature technique 6 GPa and 1470–1570 K. Synthesis time did not exceed 10 min. Details of the precursor preparation and the high-pressure synthesis can be found in Ref. [25].

The microstructural characterization of the ceramics before and after annealing was performed using a Hitachi S-4100 scanning electron microscope (SEM) (Hitachi, Chiyoda, Japan) operated at 25 kV.

To characterize the phase content and the crystal structure of the samples via X-ray diffraction (XRD), the as-prepared ceramics were reduced into fine powders. XRD measurements were performed using a PANalytical X'Pert Powder diffractometer (Malvern Panalytical, Malvern, UK) (Ni filtered Cu Kα radiation, an exposition of about 2 s per 0.02° step over a 2-theta range of 15–85°). In situ temperature-dependent XRD measurements were carried out in an Anton Paar HTK 16 N chamber between 300 and 820–1020 K upon both heating and cooling. The samples (in powder form) were kept for 30 min at each

temperature point before the XRD data collection to ensure equilibrium condition. The obtained XRD data were refined by the Rietveld method using the FULLPROF 7.60 package (Rennes-Grenoble, France) [26].

Piezoresponse force microscopy (PFM) studies were performed using a commercial scanning probe microscope MFP-3D (Asylum Research, Oxford Instruments, Santa Barbara, CA, USA). Pt coated cantilevers Multi75E-G (Budget Sensors, Sofia, Bulgaria) with a spring constant of 3 N/m were used. The PFM measurements were conducted at probing voltage with an amplitude U_{ac} = 5 V and a frequency close to the contact resonance frequency of the cantilevers (f~380 kHz and 700 kHz for the vertical and lateral PFM signals, respectively). The PFM images were analyzed using the Gwyddion 2.45 software (Gwyddion, Brno, Czech Republic) [27].

3. Results and Discussion

All the perovskite compositions of the (1-x)BMT–xBZT system were prepared using high-pressure synthesis [23]; the attempts to produce these materials via conventional ceramics methods resulted in the formation of a mixture of non-perovskite phases [25]. To estimate the thermal stability of the obtained materials at ambient pressure, high-pressure synthesized samples were thermally treated (annealed) in air and their phase transformation(s) were controlled in situ using a high-temperature XRD chamber. The maximum temperature was 1020 K. The thermal stability limit was defined as the temperature which is 50 K lower than that when the diffraction reflections of a non-perovskite phase ($Bi_4Ti_3O_{12}$) appear or start to increase. The stability limit of perovskite phases in the (1-x)BMT–xBZT system was found to depend on the BZT content and decreases as x increases (Table 1). Thus, the perovskite (1-x)BMT–xBZT phases are all metastable regardless of their crystal symmetry.

Table 1. The thermal stability limit of the high-pressure synthesized perovskite phases in the (1-x)BMT–xBZT system.

The Composition Range	The Thermal Stability Limit, K
$x \leq 0.20$	970
$0.20 < x \leq 0.65$	870
$x > 0.65$	820

SEM study has revealed no regular change in morphology of the ceramics dependent on their composition. The microstructure of a 0.30BMT–0.70BZT sample shown in Figure 1a is typical of all the ceramics under study. Annealing of the samples at temperatures below the thermal stability limit of their perovskite phase(s) was found to lead to no visible change of their microstructure (cf: Figure 1b). However, even a relatively short (about 20 min) thermal treatment at higher temperatures resulted in a drastic modification of the sample morphology (Figure 1c). The phase content of the ceramics after the decomposition of the perovskite phase was essentially similar to that of the synthesis product of samples of the same composition at ambient pressure.

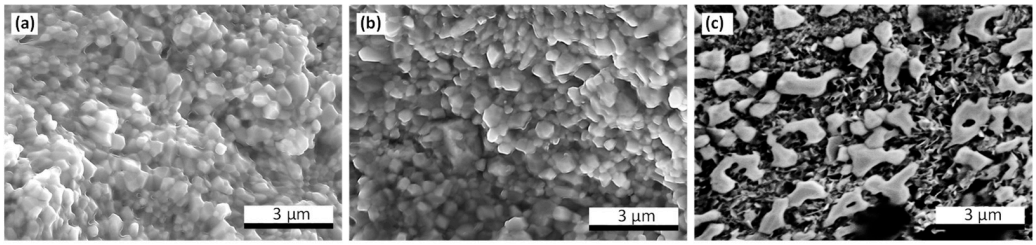

Figure 1. SEM images of the fractured surfaces of the (1-x)BMT–xBZT sample (x = 0.70) synthesized under high pressure: (**a**) as prepared, (**b**) annealed at 770 K and (**c**) annealed at 970 K.

An in situ temperature XRD study of the (1-x)BMT–xBZT solid solutions carried out at temperatures below the thermal stability limits revealed irreversible structural transitions of the perovskite phases over a wide compositional range. The orthorhombic structure of the as-prepared (unannealed) samples with $0.60 \leq x \leq 0.75$ transforms into the tetragonal structure upon heating and this structure remains upon cooling down to room temperature. Figure 2 shows the XRD patterns that demonstrate such a transformation in a sample with $x = 0.70$.

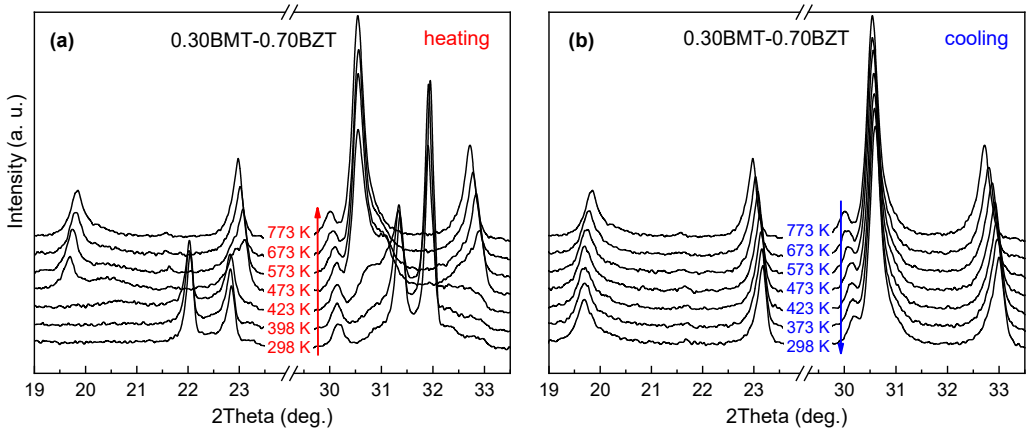

Figure 2. The most representative ranges of the XRD patterns of the as-prepared (1-x)BMT–xBZT sample ($x = 0.70$) at the first thermal cycle: (**a**) upon heating to 773 K and (**b**) upon cooling to room temperature. The structural phases at room temperature before and after the annealing are the orthorhombic *Pnnm* and the tetragonal *P*4*mm*, respectively.

For all the solid solutions from the aforementioned composition range, the transition starts at about 470 K and completes at 520–570 K. The orthorhombic structure of the unannealed samples from the range of $0.20 \leq x \leq 0.60$ transforms irreversibly to the rhombohedral structure. For these compositions, the transition initiation temperature is close to 420 K, and the phase coexistence range is about 100 K. The characteristic evolution of the XRD pattern is shown in Figure 3 for the case of a solid solution with $x = 0.40$.

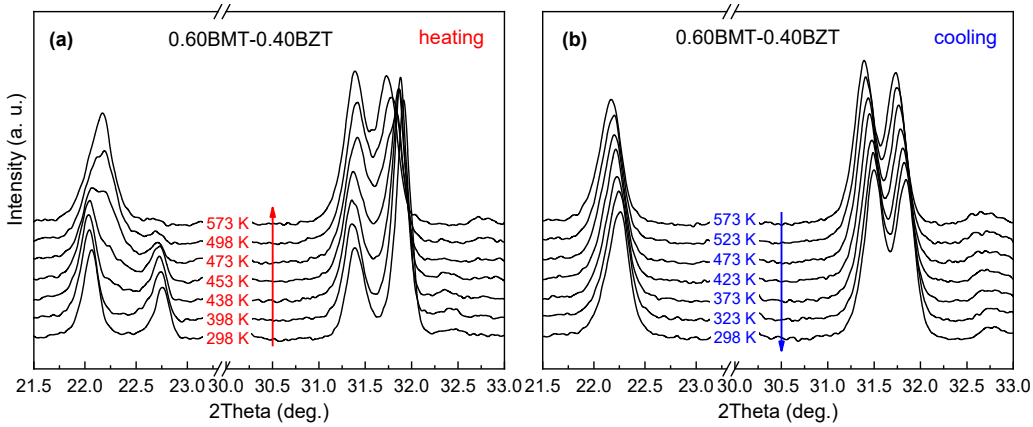

Figure 3. The most representative ranges of the XRD patterns of the as-prepared (1-x)BMT–xBZT sample ($x = 0.40$) at the first thermal cycle: (**a**) upon heating to 773 K and (**b**) upon cooling to room temperature. The structural phases at room temperature before and after the annealing are the orthorhombic *Pnnm* and the tetragonal *R*3*c*, respectively.

The (1-x)BMT–xBZT solid solutions with $x \leq 0.10$ keep the orthorhombic structure over the annealing.

Based on the results of in situ temperature XRD study, the phase diagrams of the as-prepared (1-*x*)BMT–*x*BZT perovskite compositions upon heating (Figure 4a) and cooling (Figure 4b) were plotted.

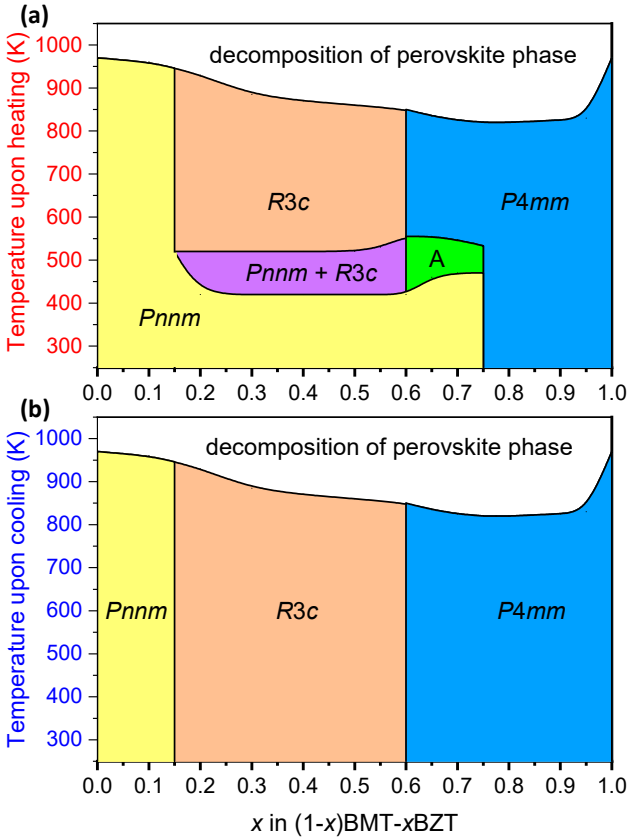

Figure 4. State diagram of the (1-*x*)BMT–*x*BZT perovskite phases upon heating to their temperature stability limit (**a**) and upon subsequent cooling (**b**). The area marked as "A" corresponds to the *Pnnm* + *P*4*mm* phase mixture.

The second and all subsequent heating/cooling thermal cycles of the annealed (1-*x*)BMT–*x*BZT samples with a maximum temperature not exceeding their temperature stability limit have demonstrated neither reversible nor irreversible structural transformation. The phase diagram of the annealed samples remained the same upon both heating and cooling (Figure 4b).

The crystal structure of the observed perovskite phases was successfully refined using the orthorhombic *Pnnm* space group with the $\sqrt{2}a_p \times 2a_p \times 2\sqrt{2}a_p$ superstructure (where a_p is the pseudocubic primitive perovskite unit-cell parameter), the rhombohedral *R*3*c* group ($\sqrt{2}a_p \times \sqrt{2}a_p \times 2\sqrt{3}a_p$) and the tetragonal *P*4*mm* group ($a_p \times a_p \times a_p$). As pointed out in Ref. [21], due to close to tetragonal metric of the pseudocubic perovskite cell, it is difficult to establish the right space group unambiguously for the orthorhombic phase, and the symmetry might be *Pnma* instead of *Pnnm*. The secondary phase identified as the orthorhombic $Bi_4Ti_3O_{12}$ [28] (space group *B*2*cb*), which was found to be present as 3–5 mol. % impurity [23], was also taken into consideration.

Figure 5 demonstrates the compositional dependence of the normalized perovskite unit-cell volume ($V_p = V/Z$) of the (1-*x*)BMT–*x*BZT solid solutions before and after annealing. It is clearly seen that except for the case of the BMT end member ($x = 0$), in the ranges where no transformation occurred ($0 < x \leq 0.1$ and $0.75 \leq x \leq 1$) as well as where the orthorhombic phase transformed into the tetragonal one ($0.60 \leq x < 0.75$), the annealing resulted in an increase of the V_p value.

It is interesting that the $V_p(x)$ dependence in the ranges of the annealed orthorhombic and the annealed tetragonal phases obeys well the linear Vegard's law and increases as x is increased (solid line in Figure 5). At the same time, in the compositional range between x = 0.20 and 0.60, where the irreversible orthorhombic-to-rhombohedral transition occurred, the unit-cell volume changes slowly and exhibits the trend to decrease with increasing x. Such an unusual behavior suggests the dominant role of the covalent bonds over the electrostatic interactions and the local crystal structure distortions in this range of the system that can result in interesting combinations of polar and elastic ferroic orders.

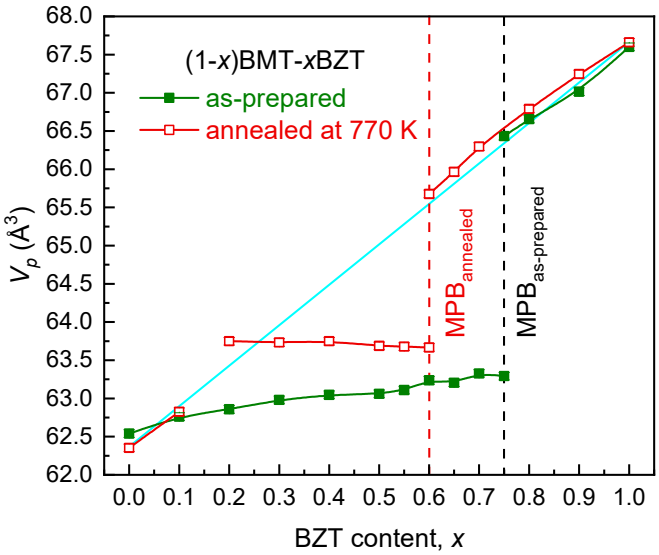

Figure 5. The normalized unit-cell volume of the (1-x)BMT–xBZT perovskite phases before and after annealing as a function of the BZT content (x). The error bars are smaller than the symbols. The dashed lines indicate the compositions corresponding to the morphotropic phase boundary (MPB) before and after annealing. The solid straight line is a reference to the Vegard's law.

The new location of the MPB in the (1-x)BMT–xBZT system, where the rhombohedral and the tetragonal phases coexist, is at x = 0.60. Thus, annealing resulted not only in the orthorhombic-to-rhombohedral transformation in the vicinity of the MPB but also in a compositional shift of the boundary by 15 mol. % in the direction of a lower BZT content. A relative jump in the V_p value upon crossing the MPB with increasing x was estimated to be about 3% as compared with 5% observed in the as-prepared (1-x)BMT–xBZT solid solutions.

The refined lattice parameters of the annealed samples with the *Pnnm* phase and the *R*3*c* phase were recalculated to the values of the primitive perovskite lattice parameters: $a_p = b_p \neq c_p$, $\alpha_p = \beta_p = 90° \neq \gamma_p$ and $a_p = b_p = c_p$, $\alpha_p = \beta_p = \gamma_p \neq 90°$ for the orthorhombic and the rhombohedral compositions, respectively [29]. The obtained values were plotted together with the $a_p(x)$ and $c_p(x)$ parameters of the tetragonal compositions for comparison. Figure 6 shows the compositional dependences of the primitive perovskite unit-cell parameters of the (1-x)BMT–xBZT solid solutions before and after the annealing.

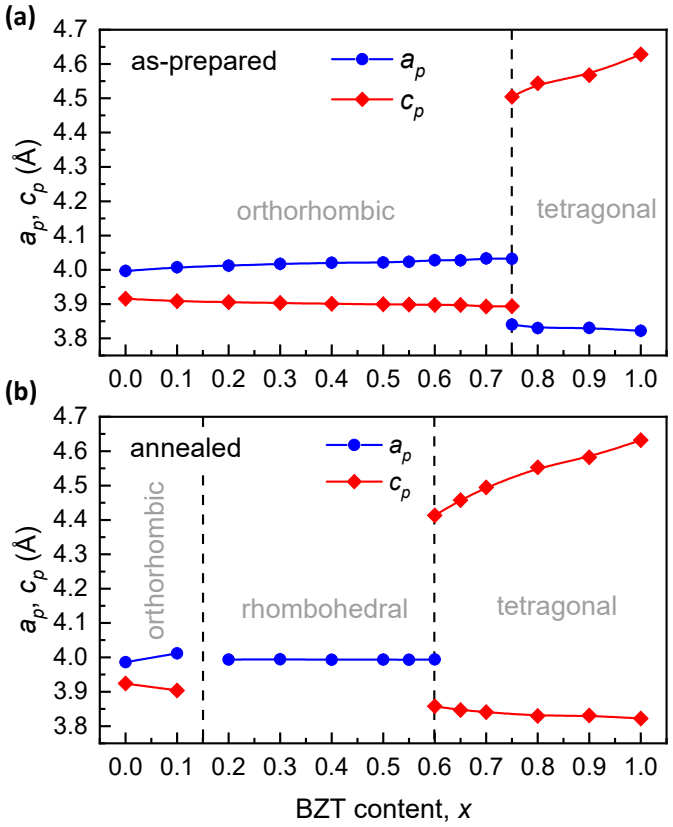

Figure 6. The primitive perovskite cell parameters of the (1-*x*)BMT–*x*BZT perovskite phases as a function of the BZT content (*x*) before (**a**) and after (**b**) annealing with the borders of the different phase ranges indicated.

The compositional dependence of the pseudocubic primitive perovskite unit-cell parameters is essentially similar to that of PZT [1].

The change in symmetry should be reflected in changes of the functional properties of the (1-*x*)BMT–*x*BZT ceramics, namely in the onset of the ferroelectric behavior. Unfortunately, small and brittle samples obtained after the high-pressure synthesis are unsuitable for macroscopic ferroelectric measurements. Nevertheless, ferroelectricity in such samples can be probed at the local scale using piezoresponse force microscopy [30]. Recently, we reported on the domain structure and local ferroelectric properties in the as-prepared (1-*x*)BMT–*x*BZT ceramics with compositions around the MPB that was detected at $x = 0.75$ [23]. In this study we focus on the compositions from the BMT-side to the MPB, with $x = 0.55$–0.70. Figures 7a–c and 8a–c show the PFM images of as-prepared ceramics with $x = 0.55$ and 0.65. Vertical PFM images for other compositions are compared in Figure S1. The images are presented in false colors, where the dark and bright contrast correspond to regions with small and large piezoresponse, respectively. One can see that, for the as prepared samples, most of the area shows a negligible piezoresponse in agreement with the non-polar macroscopic symmetry of the orthorhombic phase. However, some piezoactive regions are observed. These regions can be attributed to ferroelectric domains of the tetragonal phase similar to one in the compositions from the BZT side. The area occupied by these piezoactive domains increases in the composition with larger *x*, i.e., upon approaching the MPB.

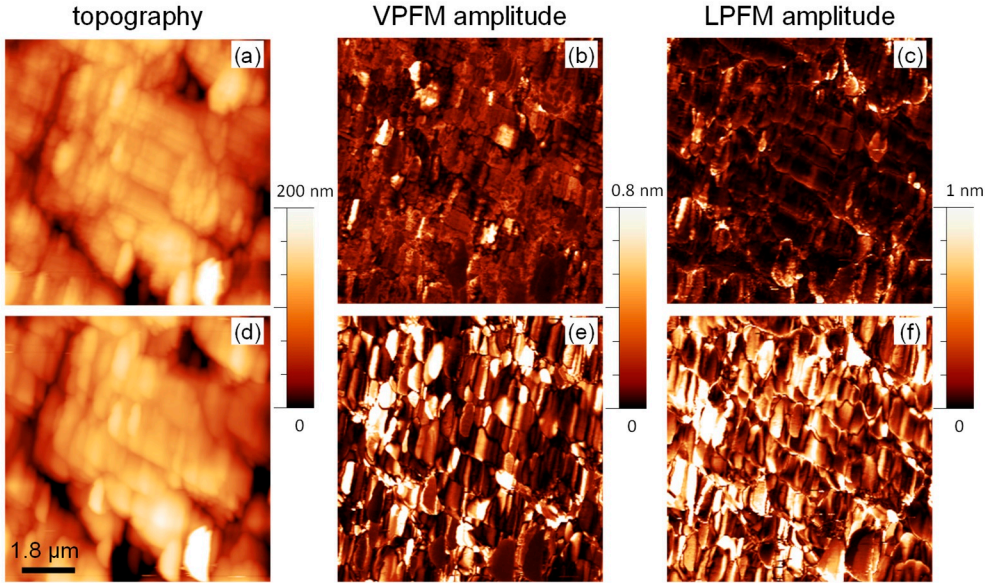

Figure 7. Topography (**a**,**d**), vertical PFM amplitude (**b**,**e**), and lateral PFM amplitude (**c**,**f**) images of the 0.45BMT–0.55BZT ceramics before (**a**–**c**) and after annealing (**d**–**f**).

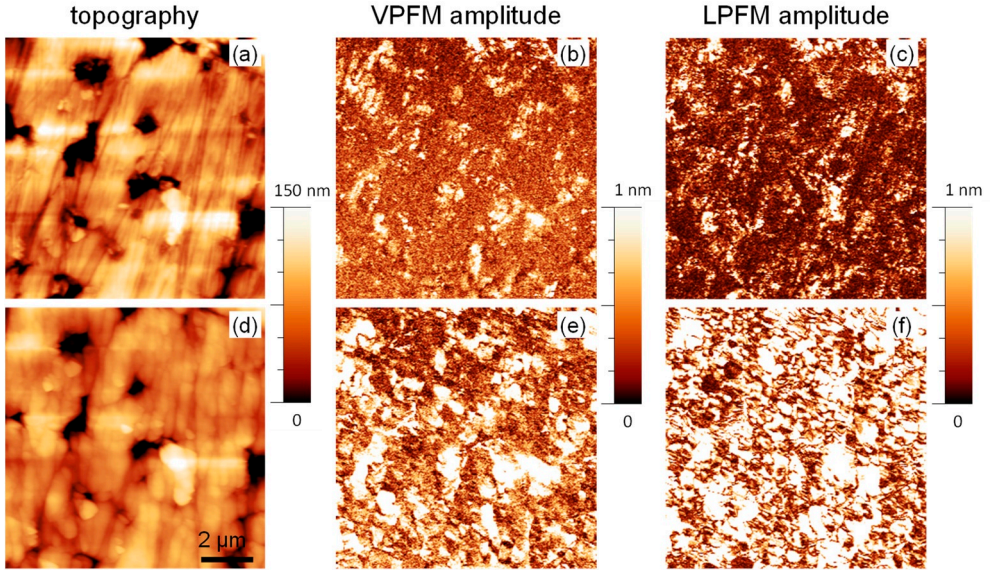

Figure 8. Topography (**a**,**d**), vertical PFM amplitude (**b**,**e**), and lateral PFM amplitude (**c**,**f**) images of the 0.35BMT–0.65BZT ceramics before (**a**–**c**) and after annealing (**d**–**f**).

Annealing results in drastic changes in the PFM images. Figures 7d–f and 8d–f show PFM images of the same areas of 0.45BMT–0.55BZT and 0.35BMT–0.65BZT ceramics taken after ex situ annealing at 623 K for 1 h.

It can be seen that regions of the strong piezoresponse increased drastically and occupied almost the whole studied area. The statistical analysis showed that the relative area occupied by the ferroelectric regions increases approximately by a factor of 6 or 7. This observation confirms that the annealing resulted in a transformation of the initially non-polar material into the polar one. We observed both growth of already existing ferroelectric domains and the appearance of new ones. This can be clearly seen in the magnified PFM images (Figure S2). It has to be noted that the domains in the annealed ceramics with x = 0.55 and 0.65 have different morphology. While in the 0.35BMT–0.65BZT ceramics, fine domains with irregular shape are observed after annealing, in the annealed 0.45BMT–0.55BZT ceramics, the domains are larger and with more regular orientation.

This may be due to the different crystalline symmetry of the annealed state, tetragonal and rhombohedral in the former and later cases, respectively.

4. Conclusions

The perovskite (1-x)$BiMg_{0.5}Ti_{0.5}O_3$–$xBiZn_{0.5}Ti_{0.5}O_3$ system is an interesting example of conversion polymorphism. The solid solutions of this system, prepared by high-pressure synthesis, have a phase diagram with an MPB between the non-polar orthorhombic and polar tetragonal phases at x = 0.75. Annealing at temperatures above 573 K leads both to an irreversible transition of compositions with $0.2 < x < 0.6$ to the polar rhombohedral state and to a shift of the morphotropic phase boundary with the tetragonal state towards the BMT-side (x = 0.6). The transformation from the non-ferroelectric to the ferroelectric state with a strong piezoelectric signal is confirmed by PFM measurements. The phase diagram of the annealed ceramics is very similar to that of the famous lead zirconate titanate ceramics, which dominate the market for piezoelectric applications but need to be replaced by environmentally friendly lead-free systems. The results obtained allow us to state that the BMT–BZT system is promising for the creation of materials with high electromechanical and dielectric characteristics.

Supplementary Materials: The following supporting information can be downloaded at: https://www.mdpi.com/article/10.3390/ma15196998/s1, Figure S1: Topography and vertical PFM amplitude images of as-synthesized (1-x)$BiMg_{0.5}Ti_{0.5}O_3$-$xBiZn_{0.5}Ti_{0.5}O_3$ ceramics: x = 0.55 (a,b), 0.60 (c,d), 0.65 (e,f), 0.70 (g,h); Figure S2. PFM amplitude images of as-synthesized $0.45BiMg_{0.5}Ti_{0.5}O_3$–$0.55BiZn_{0.5}Ti_{0.5}O_3$ (a,b) and $0.35BiMg_{0.5}Ti_{0.5}O_3$–$0.65BiZn_{0.5}Ti_{0.5}O_3$ (c,d) ceramics before (a,c) and after (b,d) annealing. White circles mark the same locations in the as-prepared and annealed ceramics.

Author Contributions: Conceptualization, A.N.S., V.V.S., D.D.K. and E.Č.; data curation, J.P.V.C., E.Č., Y.V.R. and A.V.P.; formal analysis J.P.V.C. and E.Č.; investigation, J.P.V.C., Y.V.R., A.V.P. and A.N.S.; methodology, V.V.S., D.D.K. and A.N.S.; project administration, E.Č. and N.M.O.; resources, A.F. and V.V.S.; supervision, V.V.S., A.F. and A.N.S.; validation, N.M.O. and V.V.S.; visualization, J.P.V.C., V.V.S. and A.N.S.; writing—original draft, A.N.S. and V.V.S.; writing—review and editing, J.P.V.C., V.V.S., E.Č., D.D.K., A.F. and A.N.S. All authors have read and agreed to the published version of the manuscript.

Funding: This research was funded by the bilateral Slovakia-Belarus project "Novel environment-friendly materials for microelectronics based on complex bismuth-containing oxides with perovskite structure synthesized under high pressure" through grants APVV-SK-BY-RD-19-0008 and T20SLKG-001, respectively. A.N.S. and V.V.S. acknowledge the support of the bilateral Portugal-Germany (FCT-DAAD) project PZT-FREE (grants 2021.09702.CBM and 57610755, respectively). J.P.C. was funded by the FCT—Portuguese Foundation for Science and Technology for the PhD grant SFRH/BD/145281/2019. The research done in the University of Aveiro was supported by the project CICECO-Aveiro Institute of Materials, UIDB/50011/2020, UIDP/50011/2020 & LA/P/0006/2020, financed by national funds through the FCT/MEC (PIDDAC).

Institutional Review Board Statement: Not applicable.

Informed Consent Statement: Not applicable.

Data Availability Statement: The data presented in this study are available on request from the corresponding author.

Conflicts of Interest: The authors declare no conflict of interest. The funders had no role in the design of the study; in the collection, analyses, or interpretation of data; in the writing of the manuscript, or in the decision to publish the results.

References

1. Shirane, G.; Suzuki, K. Crystal structure of Pb(Zr-Ti)O_3. *J. Phys. Soc. Jpn.* **1952**, *7*, 333. [CrossRef]
2. Jaffe, B.; Roth, R.S.; Marzullo, S. Piezoelectric properties of lead zirconate-lead titanate solid-solution ceramics. *J. Appl. Phys.* **1954**, *25*, 809–810. [CrossRef]
3. Jaffe, B.; Cook, W.R.; Jaffe, H. *Piezoelectric Ceramics*, 1st ed.; Academic Press: London, UK, 1971; pp. 7–15. [CrossRef]

4. Kimura, M.; Ando, A.; Sakabe, Y. Lead Zirconate Titanate-Based Piezo-Ceramics. In *Advanced Piezoelectric Materials*, 1st ed.; Uchino, K., Ed.; Woodhead Publishing Limited: Sawston, UK, 2010; pp. 89–110. [CrossRef]
5. Noheda, B.; Cox, D.E.; Shirane, G.; Gonzalo, J.A.; Cross, L.E.; Park, S.E. A monoclinic ferroelectric phase in the $Pb(Zr_{1-x}Ti_x)O_3$ solid solution. *Appl. Phys. Lett.* **1999**, *74*, 2059–2061. [CrossRef]
6. Guo, R.; Cross, L.E.; Park, S.-E.; Noheda, B.; Cox, D.E.; Shirane, G. Origin of the high piezoelectric response in $PbZr_{1-x}Ti_xO_3$. *Phys. Rev. Lett.* **2000**, *84*, 5423–5426. [CrossRef]
7. Zhang, N.; Yokota, H.; Glazer, A.M.; Ren, Z.; Keen, D.A.; Keeble, D.S.; Thomas, P.A.; Ye, Z.G. The missing boundary in the phase diagram of $PbZr_{1-x}Ti_xO_3$. *Nat. Comm.* **2014**, *5*, 5231–5240. [CrossRef]
8. Hall, D.A. Review Nonlinearity in piezoelectric ceramics. *J. Mater. Sci.* **2001**, *36*, 4575–4601. [CrossRef]
9. Schönau, K.A.; Schmitt, L.A.; Knapp, M.; Fuess, H.; Eichel, R.A.; Kungl, H.; Hoffmann, M.J. Nanodomain structure of $Pb[Zr_{1-x}Ti_x]O_3$ at its morphotropic phase boundary: Investigations from local to average structure. *Phys. Rev. B* **2007**, *75*, 184117. [CrossRef]
10. Bovtun, V.; Veljko, S.; Kamba, S.; Petzelt, J.; Vakhrushev, S.; Yakymenko, Y.; Brinkman, K.; Setter, N. Broad-band dielectric response of $PbMg_{1/3}Nb_{2/3}O_3$ relaxor ferroelectrics: Single crystals, ceramics, and thin films. *J. Eur. Ceram. Soc.* **2006**, *26*, 2867–2875. [CrossRef]
11. Uchino, K. Relaxor Ferroelectric-Based Ceramics. In *Advanced Piezoelectric Materials*, 1st ed.; Uchino, K., Ed.; Woodhead Publishing Limited: Sawston, UK, 2010; pp. 111–129. [CrossRef]
12. Takenaka, T. Lead-Free Piezo-Ceramics. In *Advanced Piezoelectric Materials*, 1st ed.; Uchino, K., Ed.; Woodhead Publishing Limited: Sawston, UK, 2010; pp. 130–170. [CrossRef]
13. Wang, W.; Tang, X.G.; Jiang, Y.P.; Liu, Q.X.; Li, W.H.; Guo, X.B.; Tang, Z.H. Modified relaxor ferroelectrics in $BiFeO_3$-(Ba,Sr)TiO_3-$BiScO_3$ ceramics for energy storage applications. *Sustain. Mater. Technol.* **2002**, *32*, e00428. [CrossRef]
14. Djahmoum, M.; El Kechai, O.; Marchet, P. Elaboration and characterization of materials from the $LaMnO_3$-$BiMnO_3$ binary system. *Phys. Status Solidi A* **2020**, *217*, 1900814. [CrossRef]
15. Selvamani, R.; Singh, G.; Sathe, V.; Tiwari, V.S.; Gupta, P.K. Dielectric, structural and Raman studies on $(Na_{0.5}Bi_{0.5}TiO_3)_{(1-x)}(BiCrO_3)_x$ ceramic. *J. Phys. Condens. Matter* **2011**, *23*, 055901. [CrossRef]
16. Azuma, M.; Niitaka, S.; Hayashi, N.; Oka, K.; Takano, M.; Funakubo, H.; Shimakawa, Y. Rhombohedral–tetragonal phase boundary with high Curie temperature in (1-x)$BiCoO_3$–x$BiFeO_3$ solid solution. *Jpn. J. Appl. Phys.* **2008**, *47*, 7579–7581. [CrossRef]
17. Oka, K.; Koyama, T.; Ozaaki, T.; Mori, S.; Shimakawa, Y.; Azuma, M. Polarization rotation in the monoclinic perovskite $BiCo_{1-x}Fe_xO_3$. *Angew. Chem.* **2012**, *124*, 8101–8104. [CrossRef]
18. Pan, Z.; Chen, J.; Yu, R.; Yamamoto, H.; Rong, Y.; Hu, L.; Li, Q.; Lin, K.; You, L.; Zhao, K.; et al. Giant polarization and high temperature monoclinic phase in a lead-free perovskite of $Bi(Zn_{0.5}Ti_{0.5})O_3$-$BiFeO_3$. *Inorg. Chem.* **2016**, *55*, 9513–9516. [CrossRef]
19. Pan, Z.; Nishikubo, T.; Sakai, Y.; Yamamoto, T.; Kawaguchi, S.; Azuma, M. Observation of stabilized monoclinic phase as a "bridge" at the morphotropic phase boundary between tetragonal perovskite $PbVO_3$ and rhombohedral $BiFeO_3$. *Chem. Mater.* **2020**, *32*, 3615–3620. [CrossRef]
20. Pan, Z.; Zhang, M.H.; Nishikubo, T.; Sakai, Y.; Yamamoto, H.; Hojo, H.; Fukuda, M.; Hu, L.; Ishizaki, H.; Kaneko, S.; et al. Polarization rotation at morphotropic phase boundary in new lead-free $Na_{1/2}Bi_{1/2}V_{1-x}Ti_xO_3$ piezoceramics. *ACS Appl. Mater. Interfaces* **2021**, *13*, 5208–5215. [CrossRef]
21. Khalyavin, D.D.; Salak, A.N.; Vyshatko, N.P.; Lopes, A.B.; Olekhnovich, N.M.; Pushkarev, A.V.; Maroz, I.I.; Radyush, Y.V. Crystal structure of metastable perovskite $Bi(Mg_{1/2}Ti_{1/2})O_3$: Bi-based structural analogue of antiferroelectric $PbZrO_3$. *Chem. Mater.* **2006**, *18*, 5104–5110. [CrossRef]
22. Suchomel, M.R.; Fogg, A.M.; Allix, M.; Niu, H.; Claridge, J.B.; Rosseinsky, M.J. Bi_2ZnTiO_6: A lead-free closed-shell polar perovskite with a calculated ionic polarization of 150 $\mu C.cm^{-2}$. *Chem. Mater.* **2006**, *18*, 4987–4989. [CrossRef]
23. Salak, A.N.; Shvartsman, V.V.; Cardoso, J.P.; Pushkarev, A.V.; Radyush, Y.V.; Olekhnovich, N.M.; Khalyavin, D.D.; Vieira, J.M.; Čižmár, E.; Feher, A. The orthorhombic-tetragonal morphotropic phase boundary in high-pressure synthesized $BiMg_{0.5}Ti_{0.5}O_3$-$BiZn_{0.5}Ti_{0.5}O_3$ perovskite solid solutions. *J. Phys. Chem. Solids* **2022**, *161*, 110392. [CrossRef]
24. Khalyavin, D.D.; Salak, A.N.; Fertman, E.L.; Kotlyar, O.V.; Eardley, E.; Olekhnovich, N.M.; Pushkarev, A.V.; Radyush, Y.V.; Fedorchenko, A.V.; Desnenko, V.A.; et al. The phenomenon of conversion polymorphism in Bi-containing metastable perovskites. *Chem. Commun.* **2019**, *55*, 4683–4686. [CrossRef]
25. Pushkarev, A.V.; Olekhnovich, N.M.; Radyush, Y.V. High-pressure $Bi(Mg_{1-x}Zn_x)_{1/2}Ti_{1/2}O_3$ perovskite solid solutions. *Inorg. Mater.* **2011**, *47*, 1116–1119. [CrossRef]
26. Rodriguez-Carvajal, J. Recent advances in magnetic structure determination by neutron powder diffraction. *Physica B: Condens. Matter* **1993**, *192*, 55–69. [CrossRef]
27. Nečas, D.; Klapetek, P. Gwyddion: An open-source software for SPM data analysis. *Cent. Eur. J. Phys.* **2012**, *10*, 181–188. [CrossRef]
28. Oh, S.J.; Shin, Y.; Tran, T.T.; Lee, D.W.; Yoon, A.; Shiv, H.P.; Ok, K.M. Structure–property relationships in solid solutions of noncentrosymmetric Aurivillius phases, $Bi_{4-x}La_xTi_3O_{12}$ (x = 0–0.75). *Inorg. Chem.* **2012**, *51*, 10402–10407. [CrossRef]

29. Salak, A.N.; Khalyavin, D.D.; Mantas, P.Q.; Senos, A.M.R.; Ferreira, V.M. Structure-dependent microwave dielectric properties of $(1-x)La(Mg_{1/2}Ti_{1/2})O_3–xLa_{2/3}TiO_3$ ceramics. *J. Appl. Phys.* **2005**, *98*, 034101. [CrossRef]
30. Shvartsman, V.V.; Kholkin, A.L. Nanoscale Investigation of Polycrystalline Ferroelectric Materials via Piezoresponse Force Microscopy. In *Multifunctional Polycrystalline Ferroelectric Materials: Processing and Properties*; Pardo, L., Ricote, J., Eds.; Springer: Dordrecht, The Netherlands, 2011; pp. 409–468. [CrossRef]